Available online at www.sciencedirect.com
ScienceDirect
Journal of Solid State Chemistry 180 (2007) 2437–2442
JOURNAL OF SOLID STATE CHEMISTRY
www.elsevier.com/locate/jssc

From a 3D protonic conductor $VO(H_2PO_4)_2$ to a 2D cationic conductor $Li_4VO(PO_4)_2$ through lithium exchange

V. Caignaert[a,*], M. Satya Kishore[a], V. Pralong[a], B. Raveau[a], N. Creon[b], H. Fjellvåg[b]

[a]*Laboratoire CRISMAT, UMR 6508 CNRS ENSICAEN, 6 bd Maréchal Juin, 14050 CAEN Cedex 4, France*
[b]*Department of Chemistry, University of Oslo, 0315 Oslo, Norway*

Received 9 April 2007; received in revised form 10 June 2007; accepted 20 June 2007
Available online 26 June 2007

Abstract

A new phase, $Li_4VO(PO_4)_2$ was synthesized by a lithium ion exchange reaction from protonic phase, $VO(H_2PO_4)_2$. The structure was determined from neutron and synchrotron powder diffraction data. The exchange of lithium causes a stress, leading to a change in the dimensionality of the structure from 3D to 2D by the displacement of oxygen atoms. Thus, $Li_4VO(PO_4)_2$ crystallizes in $P4/n$ space group with lattice parameters $a = 8.8204(1)$ Å and $c = 8.7614(2)$ Å. It consists of double layers $[V_2P_4O_{18}]_\infty$ formed by successive chains of VO_6 octahedra and VO_5 pyramids with isolated PO_4 tetrahedra. The lithium ions located in between the layers promote mobility. Furthermore, the ionic conductivity of 10^{-4} S/cm at 550 °C for $Li_4VO(PO_4)_2$ confirms the mobility of lithium ions in the layers. On the other hand, $VO(H_2PO_4)_2$ exhibits a conductivity of 10^{-4} S/cm at room temperature due to the presence of protons in tunnels.

Keywords: Vanadophosphate; Lithium conductor; Neutron diffraction; Synchrotron diffraction; Ab initio structure; Impedance spectroscopy

1. Introduction

The growing need to save and produce energy and simultaneously to protect the environment has encouraged the development of research in two different fields: the protonic conductors, which can be used for fuel cells and sensors applications [1–4] on the one hand and electrode materials for lithium batteries [5–15], on the other hand. Among the numerous materials that have been investigated for such applications, the phosphate-based compounds are of great interest due to their low cost and absence of toxicity. Typical examples are provided by the acidic phosphates which are fast protonic conductors [16,17] and the transition metal phosphates belonging to the Nasicon family, which are potential electrode materials due to their ability to intercalate/deintercalate lithium [5,8,15]. From the view of the battery application, the vanadium phosphates are shown to be promising because of the high potential of V^{4+}/V^{5+} (~4 V) or V^{3+}/V^{4+} (~3.5 V) redox couples. In this context, several vanadium phosphates such as Nasicon $Li_3V_2(PO_4)_3$ [15], $VOPO_4$ [11,12] and $LiVOPO_4$ [12] have been studied as cathode materials for Li-ion batteries. Recently, we have synthesized a new cathode material $Li_4VO(PO_4)_2$ with an operating voltage of ~4 V and a reversible capacity of 70 mAh/g [18]. This compound was obtained from the acidic vanadium phosphate $VO(H_2PO_4)_2$ through lithium ion exchange with LiBr in hexanol. In order to understand the properties of $Li_4VO(PO_4)_2$, we have determined the structure of this phase using neutron diffraction and X-ray synchrotron radiation. We have shown herein that the lithium for proton exchange proceeds through a topotactic reaction from a 3D structure for $VO(H_2PO_4)_2$ to a 2D structure for $Li_4VO(PO_4)_2$. In the two structures, the positions of Li^+ and protons are different. Bearing in mind the mobility of the protons and lithium ions during the reaction, we have studied the ionic conductivity in those phosphates. We show that $VO(H_2PO_4)_2$ is a good protonic conductor with a conductivity of 10^{-4} S/cm at room temperature, whereas $Li_4VO(PO_4)_2$ is a cationic conductor with a conductivity of 10^{-4} S/cm at 500 °C.

*Corresponding author. Fax: +33 231 95 16 00.
E-mail address: vincent.caignaert@ensicaen.fr (V. Caignaert).

0022-4596/$ - see front matter © 2007 Elsevier Inc. All rights reserved.
doi:10.1016/j.jssc.2007.06.019

2. Experimental

$VO(H_2PO_4)_2$ was synthesized from V_2O_3 and excess H_3PO_4 in air according to the reaction $V_2O_3 + 4H_3PO_4 \rightarrow 2VO(H_2PO_4)_2 + H_2O + H_2$. The oxidation state of vanadium changes to 4+, which is the most stable state in an aqueous media. The lithium ion exchange was performed with LiBr in hexanol. The detailed synthesis procedure has been described in a previous paper [18]. The parent protonic phase, $VO(H_2PO_4)_2$, is light green in colour and with the exchange of Li^+, it turns to light blue. Samples were dissolved in diluted HNO_3 for chemical analysis. Lithium content was estimated by atomic absorption spectroscopy (Varian, SpectrAA-20). Thermogravimetric analysis (TGA) was performed in N_2 atmosphere at a heating rate of 2 °C/min (TMA 90, Setaram). Differential scanning calorimetry (DSC) studies were carried out over the temperature range 25–600 °C at a heating rate of 5 °C/min (TA instruments, DSC 2920).

Impedance measurements were carried out with an EG&G 7220 lock-in amplifier in the frequency range 10–120 kHz. Pellets were prepared by cold pressing the powder sample. Gold electrodes were deposited by vacuum evaporation. The impedance measurements were carried out at steady-state temperatures from room temperature to 900 K under an argon atmosphere.

Neutron diffraction registered at the Norwegian reactor IFR with a wavelength of 1.554 Å between 10° and 130° (2θ). The synchrotron X-ray diffraction pattern was registered at the SNBL station (Swiss Norwegian Beam Line at ESRF, Grenoble) with a wavelength of 0.499 Å between 2° and 35.5° (2θ) with a step 0.003°. The structure refinement was carried out by Rietveld method using FullProf program. Initially, a structureless profile fitting was performed. The obtained profile parameters and lattice parameters were used for subsequent Rietveld refinement.

3. Results and discussion

3.1. Structure solution

The X-ray pattern of $Li_4VO(PO_4)_2$ shows great similarity with that of the precursor $VO(H_2PO_4)_2$. The latter crystallizes in $P4/ncc$ tetragonal space group with $a = 8.9676(1)$ Å and $c = 7.9842(2)$ Å [19]. Nevertheless, there are large variations in the intensity of some reflections. In the lithiated phase, we observe the presence of some new reflections which are forbidden in the $P4/ncc$ space group of the parent protonic phase and the c/a ratio decreases. The extinction condition, $h,k,0$: $h + k = 2n + 1$, is compatible with the $P4/nmm$ and $P4/n$ space groups. The structure solution has been searched manually from the structure of $VO(H_2PO_4)_2$ and with direct methods (Expo software). We have found the same solution for V, P and O atomic positions with both methods. After the refinement of the atomic positions, we begin a combined X-ray neutron refinement with the two sets of data in order to locate the lithium positions. From the atomic absorption spectroscopy result we found about 4.0(1) lithium atoms per formula unit. Hence, we expect 16 lithium ions per unit cell. The lithium positions were searched as positive residue in X-ray Fourier difference map and negative residue in neutron Fourier difference map. A fully occupied site has been identified at $x = 0.36$, $y = 0.86$, $z = 0.31$ on the $8g$ Wyckoff site. By contrast the presence of lithium in two other Wyckoff sites viz., $2a$ and $8g$ is hardly detected. The fitting result indicates that $2a$ site is completely occupied and $8g$ is partially occupied with 0.56 Li. The reliability factor increases when we try to increase the occupancy of $8g$ site. Thus, we are able to locate the positions of 14.5 Li, which is 90% of the expected content. Due to the low scattering factor of Li for X-ray and neutron, it is difficult to locate exactly the remaining 10% of Li ions. The Rietveld refinement plots of synchrotron X-ray diffraction and neutron diffraction are shown in Fig. 1a and b respectively. The goodness of fit are $\chi^2 = 1.90$, $R_{Bragg} = 7.6\%$ and 6.0% for X-ray and neutron data, respectively. The final structural parameters and refined coordinates with thermal factors are given in Tables 1 and 2.

3.2. Structural characterization

The projected structure of $Li_4VO(PO_4)_2$along $\vec{c}$ (Fig. 2a) shows a great similarity to that of $VO(H_2PO_4)_2$ (Fig. 2b). It consists in cross-linked $[V_2P_2O_{15}]_\infty$ chains built up of VO_5 pyramids, VO_6 octahedra and PO_4 tetrahedra running along the directions [1 1 0] and [1 $\bar{1}$ 0]. In each chain, these polyhedra share their apices in such a way that each VO_5 pyramid and each VO_6 octahedron is linked to two PO_4 tetrahedra, leading to the sequence "P–V_{py}–P–V_{oc}–P…" along $\langle 1\,1\,0 \rangle$. In fact, this arrangement is quasi identical to that observed in $VO(H_2PO_4)_2$, where one observes VO_6 octahedra only instead of VO_5 pyramids, forming $[VPO_8]_\infty$ chains with the same geometry (Fig. 2b). Thus, both frameworks delimit identical tunnels running along [0 0 1]. The difference between the two structures results from the positions of lithium cations and protons in those tunnels. But, the most important difference between the two structures deals with their dimensionality. The projection of the structure of $Li_4VO(PO_4)_2$along $\vec{a}$ (Fig. 3a) shows its bidimensional character. It consists indeed in double layers of polyhedra interleaved with Li^+ cations. The two single $[VP_2O_9]_\infty$ layers, which form the double ones are linked in such a way that one VO_6 octahedron of one single layer shares one apex with one VO_5 pyramid of the other single layer and vice versa. It results in the formation of bipolyhedral units "V_2O_{10}" built up of one VO_5 pyramid and one VO_6 octahedron. In contrast, the projection of the structure of $VO(H_2PO_4)_2$along $\vec{a}$ (Fig. 3b) shows its three-dimensional character, i.e. the successive $[V_2O_9]_\infty$ layers share the corners of their VO_6 octahedra, forming $[VO_3]_\infty$octahedral chains running along $\vec{c}$. As a consequence, one observes twice more tunnels running

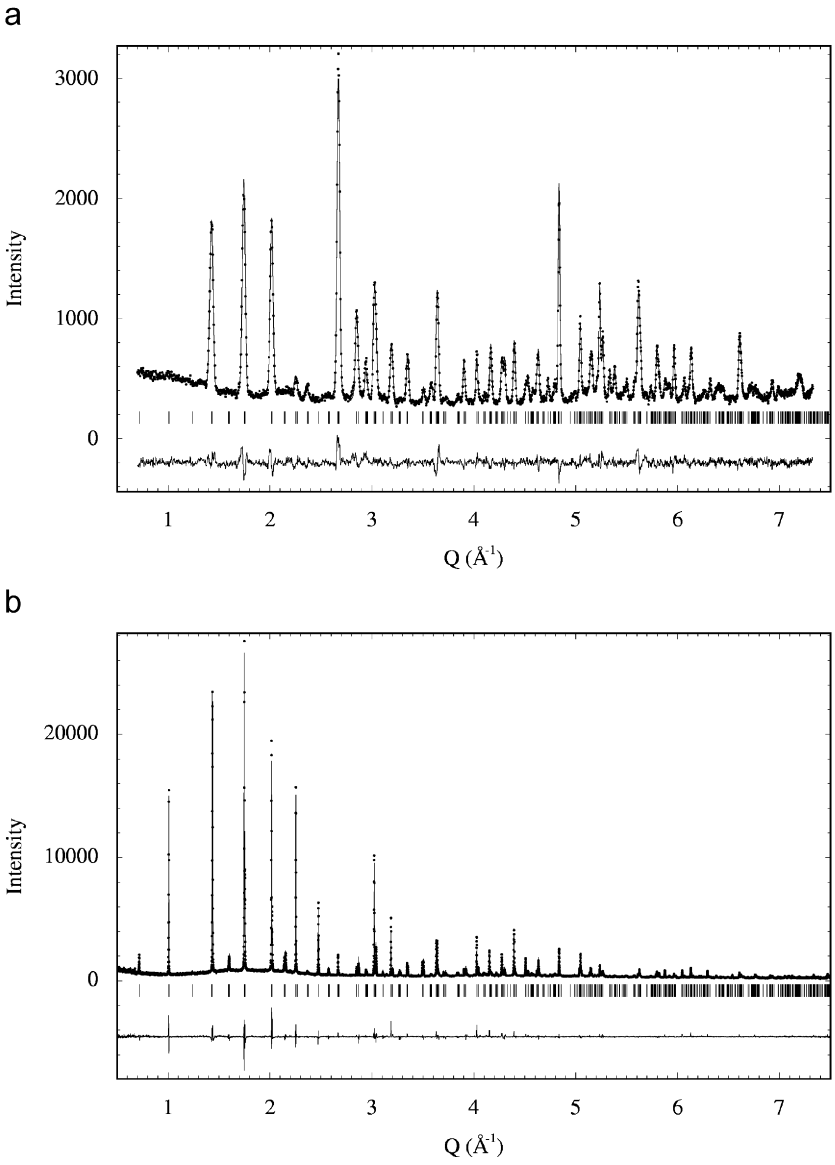

Fig. 1. Rietveld refinement plot of (a) neutron and (b) synchrotron diffraction data of $Li_4VO(PO_4)_2$.

Table 1
Structural data for $Li_4VO(PO_4)_2$

Formula sum	$Li_4VP_2O_9$
Formula weight	284.65 g/mol
Crystal system	Tetragonal
Space group	$P4/n$ (85)
Cell parameters	$a = 8.8204(1)$ Å
	$c = 8.7614(2)$ Å
Cell volume	681.64(1) Å^3
Calc. density	2.747 g/cm^3

along $\vec{a}$ or $\vec{b}$ in the $VO(H_2PO_4)_2$ structure than in $Li_4VO(PO_4)_2$.

From this structural analysis, it is apparent that the exchange of lithium for the protons is topotactic. Starting from the 3D framework of $VO(H_2PO_4)_2$, only the apical

Table 2
Fractional atomic coordinates and isotropic thermal factors for $Li_4VO(PO_4)_2$

Atom	Wyck.	S.O.F.	x/a	y/b	z/c	U [Å^2]
V1	2c	1	1/4	1/4	0.6866(5)	0.028(3)
V2	2c	1	3/4	3/4	0.7510(5)	0.020(3)
P	8g	1	0.4425(6)	0.5566(6)	0.7466(4)	0.007(1)
O1	8g	1	0.6151(11)	0.5737(12)	0.7304(6)	0.009(4)
O2	8g	1	0.4226(14)	0.3794(11)	0.7397(6)	0.017(4)
O3	8g	1	0.3643(11)	0.6325(12)	0.6149(5)	0.017(2)
O4	8g	1	0.3881(11)	0.6130(12)	0.9014(5)	0.023(3)
O5	2c	1	3/4	3/4	0.9553(12)	0.025(6)
O6	2c	1	1/4	1/4	0.4924(15)	0.027(6)
Li1	8g	1	0.359(3)	0.861(3)	0.6109(14)	0.011(6)
Li2	2a	1	1/4	3/4	0	0.014(12)
Li3	8g	0.56(6)	0.204(4)	0.034(3)	0.030(3)	0.021(20)

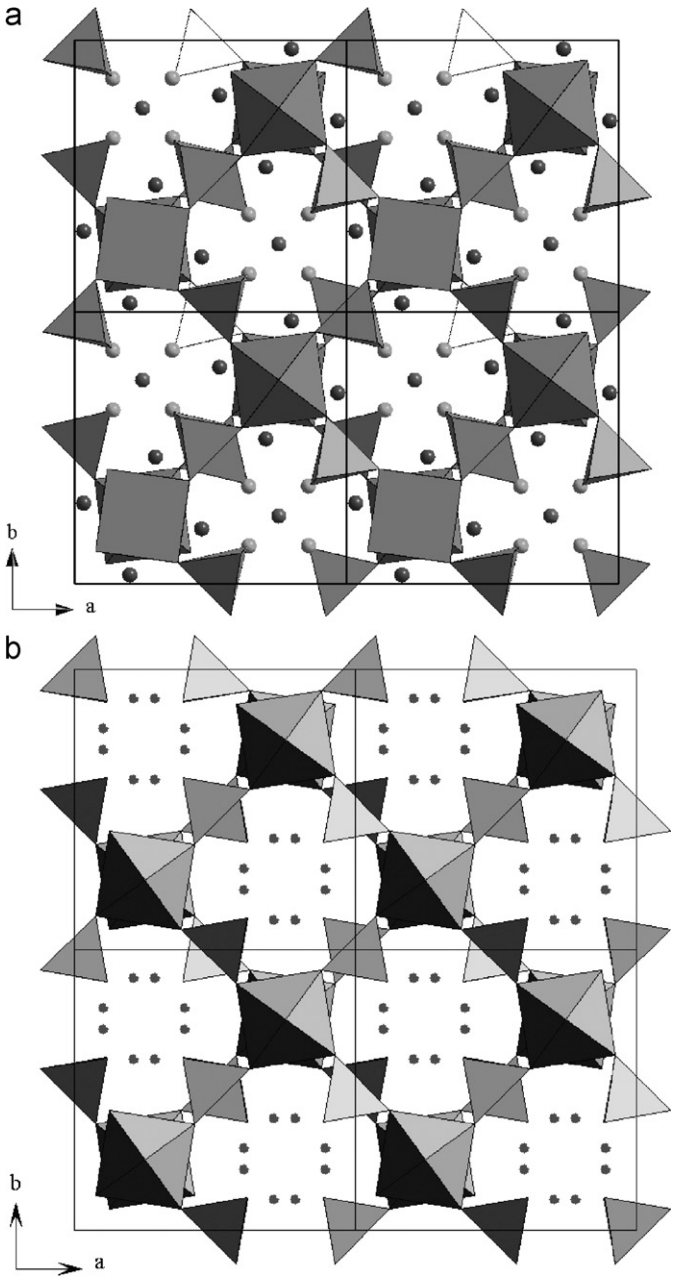

Fig. 2. Crystal structure comparison of (a) $Li_4VO(PO_4)_2$ and (b) $VO(H_2PO_4)_2$and along the $\vec{c}$ axis.

oxygen atoms of the VO_6octahedra are displaced along $\vec{c}$ during the exchange. More exactly one layer of oxygen atoms (labelled O) out of two is displaced during the exchange, whereas the second layer (labelled O') remains practically unchanged (Fig. 3b). In other words, the successive $[V_2P_4O_{18}]_\infty$ double layers of the 3D framework of $VO(H_2PO_4)_2$ are separated from each other by the introduction of lithium. At the boundary between these double layers, the oxygen atoms O5 (labelled O on Fig. 3b), are displaced towards one or the other layers (see the arrows up and down in Fig. 3b). This displacement induces a long V1–O5 distance greater than 3 Å, reducing the coordination of this vanadium to a pyramidal

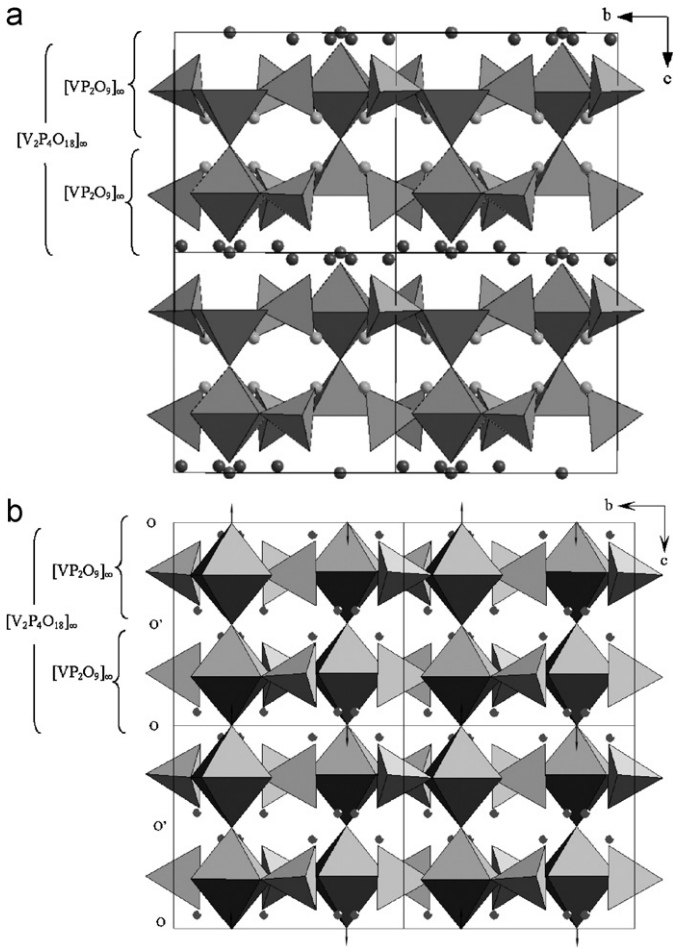

Fig. 3. Crystal structure comparison of (a) $Li_4VO(PO_4)_2$ and (b) $VO(H_2PO_4)_2$and along the $\vec{a}$ axis.

coordination. As a result, the vanadium has alternatively an octahedral and pyramidal coordination in the so formed $[VP_2O_9]_\infty$ layers of $Li_4VO(PO_4)_2$ (Fig. 3a).

The bond distances and calculated valences are given in Table 3. Vanadium V1 adopts fivefold pyramidal coordination with a short apical bond distance V1–O6 of 1.70(4) Å, whereas vanadium V2 is located in an octahedral coordination with a shift from the equatorial plane resulting in a short V2–O5 bond distance of 1.79(6) Å. The short V–O bonds are characteristic of vanadyl bond. The oxidation state calculated from bond-valence sum for V1 and V2 are 3.75 and 3.82, respectively. This confirms the presence of vanadium in +4 oxidation state. Phosphorus adopts a regular tetrahedral coordination with an average P–O bond length of 1.53 Å. Lithium ions are located in two different coordination. Li1 is found in five coordinated site with the Li–O bond distances vary between 1.97 and 2.23 Å, whereas Li2 and Li3 adopt regular and distorted tetrahedral coordination, respectively.

3.3. Thermogravimetric analysis

The TGA for $VO(H_2PO_4)_2$ sample carried out in nitrogen flow (Fig. 4) shows a large weight loss at 250 °C

in one step. As confirmed by XRPD, this weight loss is attributed to the departure of 2 mol of water, leading to the formation of VP_2O_7. On the other hand, the lithiated phase does not show any weight loss in the temperature range 25–600 °C, confirming, together with the atomic absorption analysis, the complete exchange of protons with lithium ions. The XRD pattern of the $Li_4VO(PO_4)_2$ compound heated to 600 °C indicates the decomposition of the phase into $LiVOPO_4$ and Li_3PO_4 phases according to the reaction: $Li_4VO(PO_4)_2 \rightarrow LiVOPO_4 + Li_3PO_4$. The TGA is further supported by DSC. DSC of $VO(H_2PO_4)_2$ shows a endothermic peak centred at 366 °C, which corresponds to the dehydration. Whereas, in $Li_4VO(PO_4)_2$ this peak is absent and a sharp exothermic peak is observed at 587 °C. From TGA, no accompanying mass change is observed at this temperature and this can be attributed to the phase decomposition as evidenced by the XRD.

From this analysis, we have found that the acidic vanadium phosphate is stable until 250 °C, whereas the lithiated vanadium phosphate is stable until 550 °C. Based on these findings, we have studied the ionic conductivity for these two samples.

Table 3
Selected bond distances for $Li_4VO(PO_4)_2$

		d (Å) and bonds#	Calculated valence
V1	O2	1.96(3) × 4	3.75
	O6	1.70(4) × 1	
V2	O1	1.97(3) × 4	3.82
	O5	1.79(4) × 1	
	O6	2.13(4) × 1	
P	O1	1.54(3) × 1	5.03
	O2	1.57(4) × 1	
	O3	1.50(3) × 1	
	O4	1.52(4) × 1	
Li1	O1	2.18(7) × 1	1.01
	O2	2.23(7) × 1	
	O3	2.01(8) × 1	
	O3	1.97(7) × 1	
	O3	1.98(3) × 1	
Li2	O4	1.92(3) × 4	1.17
Li3	O1	2.27(7) × 1	0.85
	O4	1.90(8) × 1	
	O4	2.15(8) × 1	
	O5	1.95(7) × 1	

3.4. Ionic conduction properties for $VO(H_2PO_4)_2$ and $Li_4VO(PO_4)_2$

The impedance plots (Nyquist) were obtained for $VO(H_2PO_4)_2$ and $Li_4VO(PO_4)_2$ between 20 Hz and 120 kHz under argon. A semi circle is observed at high frequency, followed by a spike at low-frequency region. The conductivity of acidic phosphate is $\sim 10^{-4}$ S cm^{-1} at room temperature, whereas for lithiated phosphate conductivity increases with temperature, reaching $\sim 10^{-4}$ S cm^{-1} at 550 °C.

The plot of $\log(\sigma)$ versus $1000/T$ (Fig. 5) exhibits linear feature, characteristic of the classical Arrhenius relation, $\ln(\sigma T) = \ln(\sigma_o) - E_a/k_B T$. It evidences only one regime of conductivity characterized by an activation energy $E_a = 0.23$ and 0.86 eV for $VO(H_2PO_4)_2$ and $Li_4VO(PO_4)_2$, respectively. The fact that the OH groups belonging to the monophosphate groups are bordering the tunnels in the 3D structure is strongly in favor of a protonic mobility in the structure.

On the other hand, the 2D structure of $Li_4VO(PO_4)_2$ where two lithium sites are located between the layers may promote a high mobility along the b-axis. The same range of ionic conductivity and activation energy were found for the 2D compound $Na_2VP_2O_8$ (2.12×10^{-4} S/cm at 673 K, $E_a = 0.49$ eV) [20].

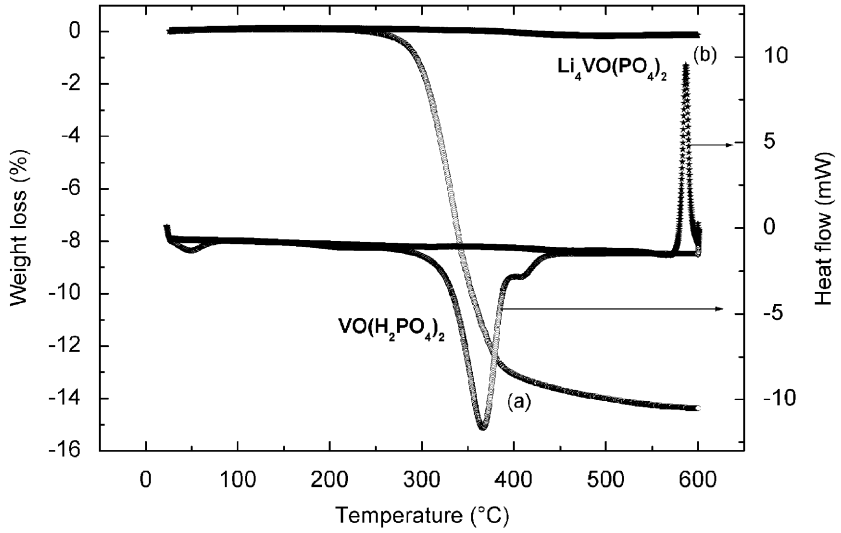

Fig. 4. TGA and DSC curves of $VO(H_2PO_4)_2$ and $Li_4VO(PO_4)_2$.

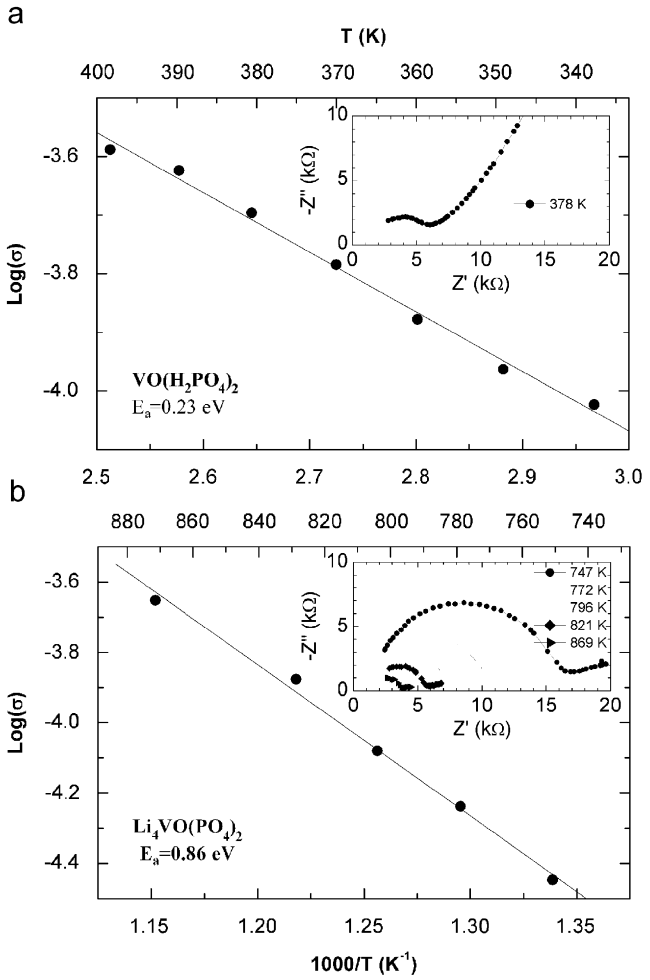

Fig. 5. (a) Arrhenius plot Log(σ) versus $1000/T$ of $VO(H_2PO_4)_2$. Inset: Nyquist plot of $VO(H_2PO_4)_2$ at 378 °C. (b) Arrhenius plot Log(σ) versus $1000/T$ of $Li_4VO(PO_4)_2$. Inset: Nyquist plots of $Li_4VO(PO_4)_2$ at various temperatures.

4. Conclusion

$Li_4VO(PO_4)_2$ is successfully synthesized by a chimie douce method. It reveals an original 2D structure formed by a double layers $[V_2P_4O_{18}]_\infty$; Li^+ are located in inter and intra layers. The mobility of the lithium between the double layers leads to a ionic conductivity of 10^{-4} S/cm at 550 °C. Anisotropy of transport measurement was not studied, however, on the basis of the underlying structures we suggest that $VO(H_2PO_4)_2$ is a 3D protonic conductor and $Li_4VO(PO_4)_2$ a 2D Li^+ conductor.

Acknowledgment

Financial support from IFCPAR (Indo-French Centre for the Promotion of Advanced Research/Centre Franco-Indien Pour la Promotion de la Recherche Avancée) is gratefully acknowledged.

References

[1] K.D. Kreuer, Chem. Mater. 8 (1996) 610.
[2] G. Alberti, M. Casciola, Solid State Ionics 145 (2001) 3.
[3] T. Norby, Solid State Ionics 125 (1999) 1.
[4] Ph. Colomban (Ed.), Proton Conductors, Cambridge University Press, Cambridge, 1992.
[5] K. Padhi, K.S. Nanjundaswamy, C. Masquelier, J.B. Goodenough, J. Electrochem. Soc. 144 (1997) 2581.
[6] K. Padhi, K.S. Nanjundaswamy, J.B. Goodenough, J. Electrochem. Soc. 144 (1997) 1188.
[7] H. Huang, S.-C. Yin, T. Kerr, N. Taylor, L.F. Nazar, Adv. Mater. 14 (2002) 1525.
[8] S.-C. Yin, H. Grondey, P. Strobel, M. Anne, L.F. Nazar, J. Am. Chem. Soc. 125 (2003) 10402.
[9] M.Y. Saïdi, J. Barker, H. Huang, J.L. Swoyer, G. Adamson, Electrochem. Solid State Lett. 5 (2002) A149.
[10] M.Y. Saïdi, J. Barker, H. Huang, J.L. Swoyer, G. Adamson, J. Power Sources 119–121 (2003) 266.
[11] N. Dupré, J. Gaubicher, T. Le Mercier, G. Wallez, J. Angenault, M. Quarton, Solid State Ionics 140 (2001) 209.
[12] B.M. Azmi, T. Ishihara, H. Nishiguchi, Y. Takita, J. Power Sources 119–121 (2003) 273.
[13] J. Barker, M. Saidi, J.L. Swoyer, J. Electrochem. Soc. 151 (2004) A796.
[14] J. Barker, M.Y. Saide, J.L. Swoyer, J. Electrochem. Soc. 150 (2003) A1394.
[15] J. Gaubicher, C. Wurm, G. Goward, C. Masquelier, L. Nazar, Chem. Mater. 12 (2000) 3240.
[16] E. Rodriguez-Castellon, J. Jimenez-Jimenez, A. Jimenez-Lopez, P. Maireles-Torres, J.R. Ramos-Barrado, D.J. Jones, J. Roziere, Solid State Ionics 125 (1999) 407.
[17] J. Otomo, N. Minagawa, C. Wen, K. Eguchi, H. Takahashi, Solid State Ionics 156 (2003) 357.
[18] M. Satya Kishore, V. Pralong, V. Caignaert, U.V. Varadaraju, B. Raveau, Electr. Commun. 8 (2006) 1558.
[19] S.A. Linde, Y.E. Gorbunova, A.V. Lavrov, V.G. Kuznetsov, Dokl. Akad. Nauk SSSR 244 (1979) 1411.
[20] Daidouh, M.L. Veiga, C. Pico, Solid State Ionics 106 (1998) 103.